Smart Mater. Struct. **23** (2014) 104011 (7pp) doi:10.1088/0964-1726/23/10/104011

Power performance improvements for high pressure ripple energy harvesting

E A Skow, K A Cunefare and A Erturk

G W Woodruff School of Mechanical Engineering, Georgia Institute of Technology, Atlanta, GA 30332-0405, USA

E-mail: eskow3@gatech.edu

Received 11 February 2014, revised 16 May 2014
Accepted for publication 23 May 2014
Published 12 September 2014

Abstract

A hydraulic pressure energy harvester (HPEH) device, which utilizes a housing in order to isolate a piezoelectric stack from the hydraulic fluid via a mechanical interface, generates power by converting the dynamic pressure within the system into electricity. Energy harvester prototypes were designed for generating low-power electricity from pressure ripples. These devices generate low-power electricity from off-resonance dynamic pressure excitation. The power produced per volume of piezoelectric material is analyzed to increase the power density; this is accomplished through evaluating piezoelectric stack characteristics, adding an inductor to the system circuit, and solving for optimal loading in order to achieve maximum power output. The prototype device utilizes a piezoelectric stack with high overall capacitance, which allows for inductance matching without using an active circuit. This work presents an electromechanical model and the experimental results of the HPEH devices using a parallel connection of inductive and resistive loads as the energy harvesting circuit. A non-ideal inductive load case is also considered and successfully modeled by accounting for the parasitic resistance of the inductive load. Various HPEH prototypes are fabricated, modeled, and compared in terms of their normalized power density levels, and milli-Watt level average power generation is demonstrated. The highest power density is reported for the single-crystal HPEH prototype.

Keywords: acoustic, piezoelectricity, hydraulics, energy harvesting

(Some figures may appear in colour only in the online journal)

1. Introduction

Hydraulic systems utilize a number of wired or battery-powered sensors, such as pressure, temperature, or health monitoring sensors; however, the system naturally contains a high energy-density pressure ripple that is otherwise unused. The pressure ripple is the acoustic pressure within hydraulic systems that is caused by pumps and actuators. The pressure ripple is analogous to the AC component of an electrical signal composed of both AC and DC components. Hydraulic pressure energy harvester (HPEH) devices have been developed to convert the pressure fluctuations into useable electric power to enable wireless sensor networks, previously introduced by Cunefare *et al* [1].

Enabling self-powered wireless electronic systems is typically the end goal for energy harvesting from ambient energy sources research [2–5]. Acoustic energy harvesting, in particular, requires a system that either has high intensity, small power requirements, or a method to focus or concentrate the energy. For example, an electromechanical Helmholtz resonator was developed by Taylor *et al* [6] to increase the pressure amplitude from an acoustic field. This was later demonstrated within the nacelle of a jet aircraft engine by Liu and Phipps *et al* [7, 8]. In addition, harvesting from pressure fluctuations through the use of piezoelectric diaphragms, in combination with a pressure chamber, has been investigated by Wang and Liu *et al* [9] and Deterre *et al* [10].

HPEH devices utilize piezoelectric stacks excited at a low dominant frequency (relative to the stack resonance frequency) within the pressure ripple. The combination of frequency of excitation and high piezoelectric capacitance (relative to the capacitance of one or two piezoelectric layers, as in typical benders) allow for the use of a shunted

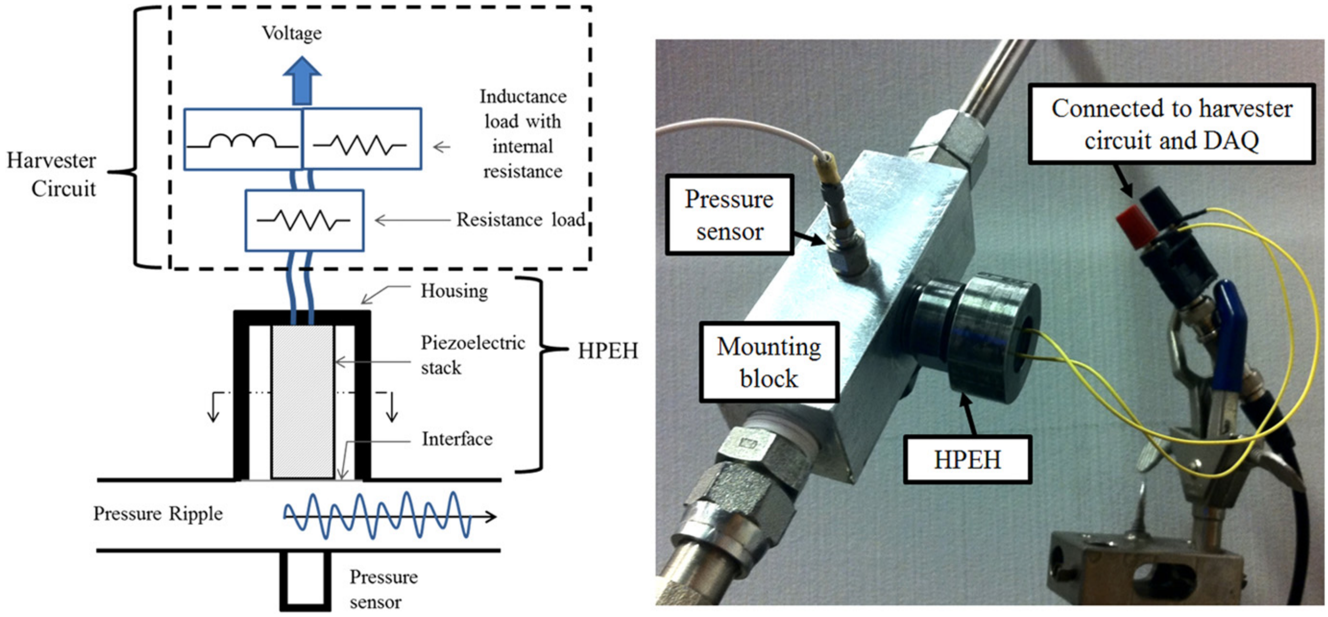

Figure 1. HPEH schematic including a resistive-inductive energy harvesting circuit and a picture of the experimental setup.

piezoelectric containing a load resistance in parallel with a load inductance. A decade before the research explosion in the energy harvesting field, Hagood and von Flotow [11] proposed using this shunt to take advantage of the electrical resonant effects with the end application providing for passive structural damping. While synthetic impedances had been introduced [12], the system parameters of HPEH devices do not require synthetic inductance or impedance. With regard to power generation with a mechanically and electrically resonant (second-order) system, Renno *et al* [13] analyzed the parallel resonant circuit and piezoelectric parameters, and he found that it was possible to maximize the power output for all excitation frequencies when using an optimal resistive and optimal inductive load. The capacitance of typical mechanically second-order piezoelectric energy harvesters, such as linear or nonlinear cantilevers [14–17], is typically low (on the order of nF), making the inductance requirement very high at ambient vibration frequencies. This is partly the reason that linear (and passive) resistive-inductive circuits have not been effectively used to date in energy harvesting literature since the theoretical work by Renno *et al* [13]. However, piezoelectric stacks used in HPEH devices have larger capacitance values than typical bimorphs or unimorphs, making linear and passive resistive-inductive loading a viable solution.

This work presents an electromechanical model for hydraulic pressure energy harvesters when using the parallel resonant shunt, including the parasitic resistance of the inductive load. The optimal resistive and inductive loads are introduced and used in an analysis to determine how HPEH piezoelectric stack parameters and hydraulic system operating conditions may change the power response. The model is then validated through comparisons to experimental results for a variety of prototype HPEH devices.

2. Hydraulic pressure energy harvesting

HPEH devices are designed to convert the noise in the fluid within a hydraulic or pumped-fluid system into usable electricity, which can then be used by sensor nodes or other low-power systems. An HPEH, shown in figure 1, has a piezoelectric stack coupled to the pressure ripple within the hydraulic system via a diaphragm interface. The piezoelectric stack is pre-compressed during operation by the mean pressure of the system, with current prototype devices designed to withstand up to 35 MPa of hydrostatic pressure. The stack is excited by the pressure fluctuations about the mean, also referred to as the pressure ripple or dynamic pressure, which can reach up to 10 percent of the mean pressure. The piezoelectric stack is connected to an energy harvesting circuit meant to maximize the electrical power output of the device before rectifying. The energy harvesting circuit parameters (resistive and inductive loads) are matched to the piezoelectric stack properties and hydraulic system operating characteristics.

The HPEH devices are tested on a hydraulic system that uses a 9 piston pump and that operates at 1500 rpm, yielding a fundamental frequency of 225 Hz. The HPEH device is connected to a mounting block that is placed in-line with the fluid flow. Opposite the HPEH device is a pressure transducer that is able to measure the dynamic pressure input to the system. The HPEH device is connected electrically in parallel to a decade resistance box and a decade inductance box. These compose the energy harvesting circuit and allow for load resistance and load inductance values to be changed with ease during testing; each inductor load that is tested has its internal resistance measured for use in the electromechanical model, which is described in the next section. The energy harvesting circuit is connected to a data acquisition system to measure the voltage response, from which power produced by

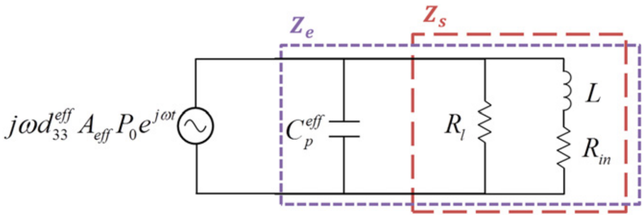

Figure 2. Circuit model for a HPEH device shunted to a resistive-inductive load with internal resistance of the inductor (current source in parallel with internal capacitance and shunt impedance).

the device can be obtained. Additional details regarding the testing of HPEH devices can be found in [1]. The next section discusses an electromechanical model of the HPEH devices using a parallel connection of inductive and resistive loads as the energy harvesting circuit.

3. Power output under resistive-inductive loading with parasitic resistance

Hydraulic pressure energy harvesting devices are well-suited for parallel resonant circuits to increase the power output of the device; however, an ideal resonant circuit does not accurately model HPEH device performance due to parasitic resistance within the inductive load. In this section, an electromechanical model of the average power produced by the HPEH device utilizing both a load resistance and inductance in parallel is introduced and a comparison to the model using an ideal inductive load and a discussion of the shunt efficiency and the optimal resistive and inductive loads is included. Resistive-reactive shunt circuits are well-known from the literature of shunt damping, e.g., Hagood and von Flotow [11]. In the energy harvesting literature, Renno *et al* [13] presented theoretical optimal conditions for a mechanically second-order system, such as resonant piezoelectric cantilevers [14, 15]. However, the HPEH configuration is a mechanically first-order system since it is excited at frequencies substantially below the fundamental mechanical resonance frequency.

If N thickness-poled layers of the HPEH stack are connected in parallel to an external shunt of impedance Z_s (see figure 2), then the governing circuit equation is obtained from

$$\sum_{i=1}^{N} \frac{\mathrm{d}}{\mathrm{d}t}\left(\int_{A_i} \mathbf{D} \cdot \mathbf{n} \mathrm{d}A_i\right) = \frac{v(t)}{Z_s}, \tag{1}$$

where $v(t)$ is the voltage response across the shunt (i.e., across the terminals of the stack), $\mathbf{D}$ is the vector of electric displacements, $\mathbf{n}$ is the vector of the surface normal of the electrodes, and the integration of their inner product is performed over the electrode area A_i of the ith layer. The nonzero contribution from the electric displacement is due to

$$D_3 = d_{33}T_3 + \varepsilon_{33}^T E_3, \tag{2}$$

where T_3 and E_3 are the stress and electric field components, respectively; d_{33} is the piezoelectric strain constant for each layer, and ε_{33}^T is the permittivity constant for each layer at constant stress. The stress component is due to the hydraulic pressure acting in the 3-direction, $T_3(t) = P_0 e^{j\omega t}$ (where P_0 is the pressure amplitude, ω is the excitation frequency, i.e., dominant hydraulic ripple frequency, and j is the unit imaginary number), and the electric field is related to the voltage across the shunt by $E_3(t) = -v(t)/h$ (where h is the thickness of each piezoelectric layer). The voltage output is also harmonic at steady state in the form of $v(t) = V_0 e^{j\omega t}$. Note that the excitation frequency ω is assumed to be much less than the fundamental resonance frequency of the stack (which is typically on the order of tens of kHz). The voltage output at steady state is then obtained from equations (1) and (2) as

$$v(t) = V_0 e^{j\omega t} = j\omega Z_e d_{33}^{eff} A_{eff} P_0 e^{j\omega t}, \tag{3}$$

where $A_{eff} = \gamma A_{stack}$ is the effective area of the interface on which the hydraulic pressure is acting, and γ is the ratio between the effective interface area (A_{eff}), protecting the stack from the fluid and the cross-sectional area ($A_{stack} = A_i$) of the stack [1] ($\gamma > 1$). Furthermore, d_{33}^{eff} is the effective piezoelectric strain constant ($d_{33}^{eff} = Nd_{33}$ under ideal fabrication conditions), and the total electrical impedance (Z_e) is

$$Z_e = \left(j\omega C_p^{eff} + \frac{1}{Z_s}\right)^{-1}, \tag{4}$$

which includes both the shunt impedance (Z_s) and the inherent effective capacitance of the stack denoted by C_p^{eff} $\left(\text{where } C_p^{eff} = N\varepsilon_{33}^T A_{stack}/h\right)$. Figure 2 illustrates the circuit elements covered by the external shunt impedance Z_s and the total electrical impedance Z_e. For an ideal shunt with resistive-inductive loading in parallel, the shunt impedance is

$$Z_s^{ideal} = \left(\frac{1}{R_l} + \frac{1}{j\omega L}\right)^{-1}, \tag{5}$$

where R_l is the load resistance, and L is the inductance (of the ideal inductor). In the presence of internal (or parasitic) resistance for the inductor, the shunt impedance becomes

$$Z_s = \left(\frac{1}{R_l} + \frac{1}{R_{in} + j\omega L}\right)^{-1}, \tag{6}$$

where R_{in} is the internal resistance of the inductor.

The average power dissipated in the resistive electrical load (R_l) can be given as

$$\Pi_{avg,l} = \frac{v_{rms}^2}{R_l} = \frac{|Z_e|^2 \left(\omega d_{33}^{eff} A_{eff} P_0\right)^2}{2R_l}, \tag{7}$$

where v_{rms} is the root-mean-square voltage, while the total power dissipated in the shunt is

$$\Pi_{avg,total} = \frac{|Z_e|^2 \left(\omega d_{33}^{eff} A_{eff} P_0\right)^2}{2\,|Z_s|^2} \mathrm{Re}\left(Z_s\right). \tag{8}$$

Using equations (7) and (8), the shunt efficiency can then be defined as

$$\eta_s = \frac{\Pi_{avg,l}}{\Pi_{avg,total}}. \tag{9}$$

For the case of an ideal inductor, i.e., $R_{in} = 0$, the power dissipated in the resistive electrical load (R_l) is

$$\Pi_{avg,l}^{ideal} = \frac{R_l \left(\omega d_{33}^{eff} A_{eff} P_{rms}\right)^2}{1 + R_l^2 \left(\omega C_p^{eff} - 1/\omega L\right)^2} \tag{10}$$

with a shunt efficiency of 100%, since no additional losses are introduced with the ideal inductor. So, $\Pi_{avg,l}^{ideal} = \Pi_{avg,total}^{ideal}$. Note that $P_{rms} = P_0/\sqrt{2}$ is the root-mean-square pressure acting on the effective area. The optimal inductance for equation (10) can be calculated as

$$\frac{\partial \Pi_{avg,l}^{ideal}}{\partial L} = 0 \rightarrow L_{opt}^{ideal} = \frac{1}{\omega^2 C_p^{eff}}, \tag{11}$$

yielding the maximum power output of

$$\Pi_{avg,l}^{ideal}\Big|_{L=L_{opt}^{ideal}} = R_l \left(\omega d_{33}^{eff} A_{eff} P_{rms}\right)^2. \tag{12}$$

Equation (12) implies that, with increasing resistance, the power will increase indefinitely, which is not physically realizable. The realistic case is the presence of a parasitic resistance for the inductor, i.e., $R_{in} \neq 0$, which is discussed next.

For the case of an inductor with parasitic resistance, the shunt impedance is given by equation (6), and the average power equations for the resistive load and the total shunt dissipation become

$$\Pi_{avg,l} = \frac{R_l \left(R_{in}^2 + \omega^2 L^2\right)\left(\omega d_{33}^{eff} A_{eff} P_{rms}\right)^2}{\left(-\omega^2 C_p^{eff} R_l L + R_l + R_{in}\right)^2 + \omega^2 \left(L + C_p^{eff} R_l R_{in}\right)^2}, \tag{13}$$

and

$$\Pi_{avg,total} = \frac{R_l \left(R_{in}^2 + R_l R_{in} + \omega^2 L^2\right)\left(\omega d_{33}^{eff} A_{eff} P_{rms}\right)^2}{\left(-\omega^2 C_p^{eff} R_l L + R_l + R_{in}\right)^2 + \omega^2 \left(L + C_p^{eff} R_l R_{in}\right)^2}. \tag{14}$$

This leads to a shunt efficiency of

$$\eta_s = \frac{R_{in}^2 + \omega^2 L^2}{R_{in}^2 + R_l R_{in} + \omega^2 L^2}. \tag{15}$$

Equation (15) suggests that the shunt efficiency approaches unity for $R_{in}^2 + \omega^2 L^2 \gg R_l R_{in}$, whereas it approaches zero for $R_{in}^2 + \omega^2 L^2 \ll R_l R_{in}$.

From equation (13), the optimal resistive load and the optimal inductor values can be obtained as

$$\frac{\partial \Pi_{avg,l}}{\partial R_l} = 0 \rightarrow R_{l,opt}, \quad \frac{\partial \Pi_{avg,l}}{\partial L} = 0 \rightarrow L_{opt}, \tag{16}$$

from which the optimal load resistance is obtained as

$$R_{l,opt} = \frac{\sqrt{(-2\omega^2 C_p^{eff} L + 1 + (\omega^2 C_p^{eff} L)^2 + (\omega C_p^{eff} R_{in})^2)(R_{in}^2 + \omega^2 L^2)}}{(-2\omega^2 C_p^{eff} L + 1 + (\omega^2 C_p^{eff} L)^2 + (\omega C_p^{eff} R_{in})^2)} \tag{17}$$

and the optimal load inductance is

$$L_{opt} = \frac{\left(R_l + 2R_{in}\right) + \sqrt{\left(R_l + 2R_{in}\right)^2 + 4\left(\omega C_p^{eff} R_l R_{in}\right)^2}}{2\omega^2 C_p^{eff} R_l}. \tag{18}$$

The ripple frequency (ω) is typically the dominant frequency in the pressure ripple; however, this parameter may be modified, depending on the type of system in which the HPEH device is to be used. It should be noted that, as the internal resistance of the inductance approaches zero, the optimal inductance for the parasitic resistance case approaches the optimal inductance for the ideal inductive load case, as previously defined in equation (11). The ideal inductive load can be used as an initial estimate for testing values, since R_{in} is usually not known before the inductive load is chosen. In the next section, an analysis of how using the optimal resistive and inductive loads in the harvested power model, equation (13), affects the power response with respect to the excitation frequency, is discussed.

4. Parameter selection and power density of HPEH devices

As can be seen in the optimal resistive and inductive load equations (17) and (18), the frequency ω, the capacitance C_p^{eff}, and the internal resistance R_{in} are the governing parameters for optimizing the power for a single excitation frequency. Other parameters that affect the power output include the piezoelectric strain constant d_{33}^{eff}, the stack volume, and the force excitation F_{rms}, or equivalently, pressure and effective area $\left(F_{rms} = P_{rms} A_{eff}\right)$. When the force, the frequency at which the force is dominant, or the piezoelectric strain constant is increased, the average power extracted by the HPEH device also increases. The optimal resistive/inductive loads and parameters affecting those loads require further analysis in order to determine their influence on the harvested power response.

The optimal resistive and inductive loads can be determined for a given piezoelectric stack when an approximate internal resistance is assumed, using equations (17) and (18). For example, the normalized power density of a piezoelectric stack can be plotted using the harvested power model with respect to load resistance and load inductance with an assumed internal resistance of 80 Ω and peak frequency of

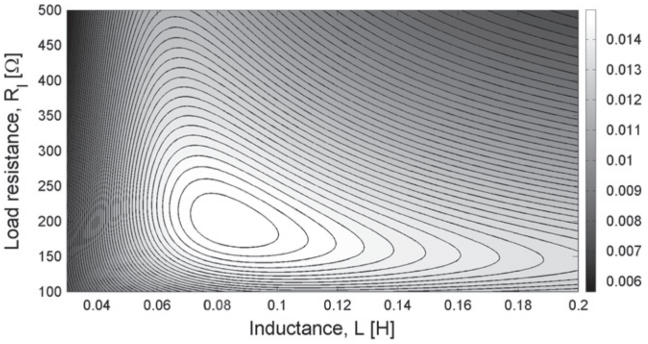

Figure 3. Normalized power density versus load resistance and inductance (for $R_{in} = 80\ \Omega$, $f = \omega/2\pi = 450$ Hz, $d_{33}^{eff} = 182.9$ nC N^{-1}, and $C_p^{eff} = 3.08\ \mu$F).

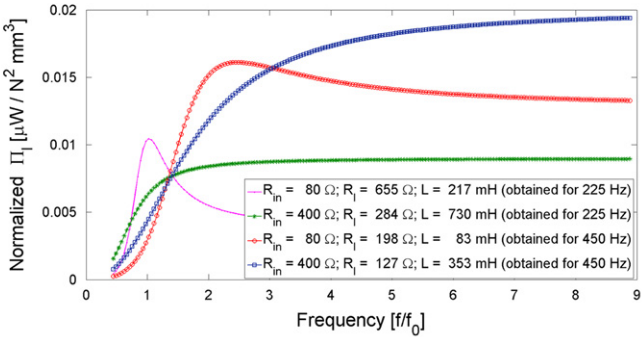

Figure 4. Normalized power versus frequency for different parameter combinations ($d_{33}^{eff} = 182.9$ nC N^{-1}, $C_p^{eff} = 3.08\ \mu$F, $f_0 = \omega_0/2\pi = 225$ Hz).

450 Hz, as shown in figure 3. When solving equations (17) and (18) simultaneously, the predicted optimal load resistance is 198 Ω, and the optimal load inductance is 83 mH, which corresponds to peak power in figure 3. This confirms that maximum power occurs at the calculated optimal loads for an assumed internal resistance and excitation frequency; however, it does not show how the harvested power changes for different assumed values.

It is of interest to explore the effect of changing circuit resonant frequency ω and internal resistance R_{in}. For instance, the hydraulic rig currently used for testing HPEH devices is set to have a fundamental operating frequency f_0 of 225 Hz; however, the dominant frequency within the pressure ripple has been shown to be the second harmonic of 450 Hz for low static pressure tests [1] and is the second dominant frequency for high static pressure tests. As can be seen in figure 4, when using optimal loads that use the higher ω value, the potential power output for the second harmonic and above is greater; however, it is very low for the fundamental frequency. The effect of the internal resistance is also shown in figure 4. It may be better to choose a device where the internal resistance will be higher if the system changes its fundamental ripple frequencies. If the system dominant pressure frequency remains focused at a single frequency, an optimal inductive load with a lower internal resistance may be better suited for the application. Note that figure 4 uses the calculated optimal resistive and inductive loads to obtain the power normalized by squared force and stack volume.

The above analysis can be used to find a balance between the system of interest and the HPEH design to meet the power response goals. It is important to also check the feasibility of the optimal resistive and inductive loads with the assumed internal resistance for a given piezoelectric when performing this analysis. As the capacitance of the stack decreases, the optimal inductive load will increase, which can be estimated by the ideal inductor optimal load from equation (11). This increase in inductive load typically corresponds to an increase in internal resistance. With the optimal loads and appropriately assumed internal resistance and excitation frequency, a desired HPEH power response for a given system can be determined.

Figure 5. HPEH devices tested in this work (from left to right: 1-2, 2, 3-1, 3-2, 4, 6, 1-3, and 5).

5. Prototype testing, comparison, and model validation

A number of HPEH prototypes have been developed, as displayed in figure 5. The devices are labeled by HPEHX-Y, in which X represents the type of piezoelectric stack, and Y, which represents a different housing design for a given stack. In the following, the model of the power produced by a HPEH device shown in equation (7) will be used in comparison to four tested prototypes: HPEH1-2, HPEH1-3, HPEH4, and HPEH6.

These devices are chosen as they represent a selection of stack volumes, piezoelectric coefficients, effective areas, and capacitances. Characteristics of the HPEH devices are shown in table 1. HPEH1-2, HPEH4, and HPEH6 are used for lower pressure ripple excitation and load inductor sweeps. HPEH1-3 and again, HPEH4, are used for higher pressure ripple excitation and load resistance sweeps.

It is of interest to understand how the prototypes perform with respect to the power normalized by force squared and volume, i.e., the normalized power, for a fair comparison. Also, the force incorporates the electrode area, HPEH device area ratio, and the dynamic pressure amplitude. Comparing

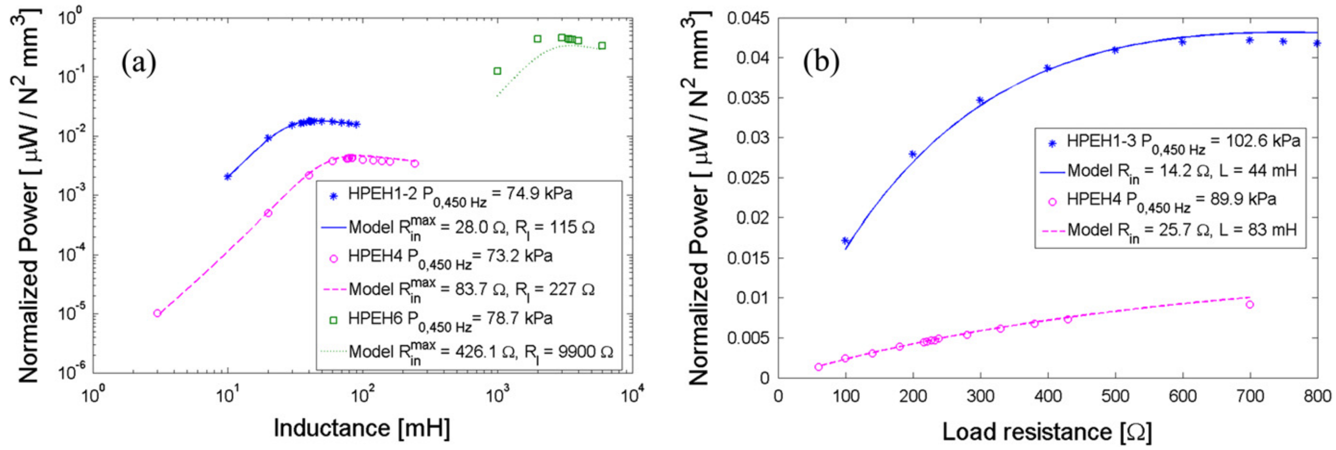

Figure 6. HPEH power delivered to the resistive load normalized by force and stack volume versus load (a) inductance and (b) resistance (ripple frequency: 450 Hz).

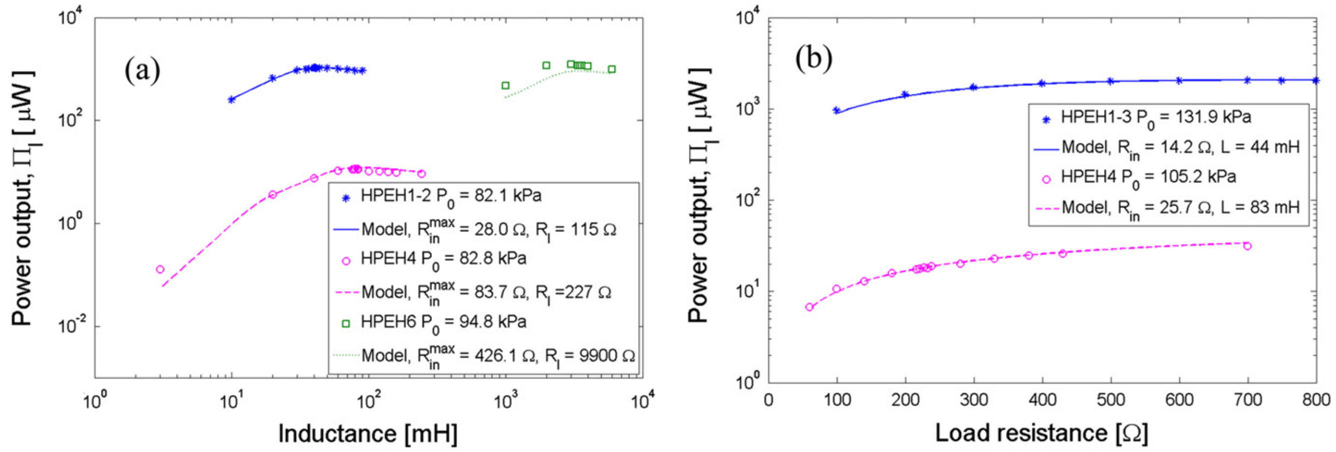

Figure 7. HPEH device power comparison for different devices versus load (a) inductance and (b) resistance.

the device performance without the volume and force effects allows the power density to be analyzed, which in turn allows the design of more compact device designs. As seen in figure 6, the HPEH1 piezoelectric stack exhibits higher power density than the HPEH4 stack. It can also be seen that the HPEH6 (single crystal) device has the highest power density. The HPEH1 devices are the largest stacks with the highest number of piezoelectric layers; however, the material properties of the single crystal HPEH6 stack are better suited for higher power output. The HPEH4 device has the smallest volume, making the overall device the smallest, in addition to producing the least overall power (figure 6(b)). The tests performed are centered around the estimated ideal optimal inductance for the piezoelectric stack when using $f = \omega/2\pi = 450$ Hz, which is the second harmonic of the pump operating frequency. The tests shown are for a single excitation frequency of 450 Hz.

The average power model for a HPEH device using a resonant circuit with parasitic resistances is compared to the measured power during resistive and inductive load sweeps in figure 7. Previous analysis of a wireless sensing device that was battery-powered required micro-Watt (67 μW sampling rate 2 times per minute) power levels, which is considered here as a base requirement power level for sensing and communication sensor nodes. While HPEH4 did not meet this power level for the given pressure levels, the other devices exceeded the power requirements. Furthermore, the HPEH4 device did meet the power requirements during a different test at a higher pressure level (near 400 kPa pressure ripple [18]). HPEH1-2 and HPEH1-3, which both use the same piezoelectric stack, produced the highest power outputs. Note that the power output for figure 7(b) is higher than figure 7(a), due in part to the higher pressure ripple. In addition, the model corresponds well with the test results for the different prototypes.

Overall, the electromechanical model is observed to predict the power generation performance of the prototypes with very good accuracy. The single-crystal HPEH6 device had the highest power density; however, the HPEH1 devices produced the higher power output due to their larger volumes.

Table 1. HPEH device stack and design characteristics.

Device	HPEH1-2	HPEH1-3	HPEH4	HPEH6
Type/manufacturer	EPCOS	EPCOS	Piezomechanik	Single crystal
Effective piezoelectric constant (d_{33}^{eff}) [nC N^{-1}]	182.93	182.93	9.39	36.15
Effective capacitance (C_p^{eff}) [nF]	3080	3080	1417	42
Stack volume [mm^3]	1387	1387	50	294
Stack height [mm]	30	30	2	11.75
Stack area (A_{stack}) [mm^2]	46.24	46.24	25	25
Design effective area (A_{eff}) [mm^2]	120	122	88	89

6. Conclusion

Hydraulic pressure energy harvesting (HPEH) devices are designed to convert the noise in the fluid within a hydraulic or pumped-fluid system into usable electricity, which can then be used by sensor nodes or other low-power systems. This paper introduced an electromechanical model for HPEH devices utilizing a resonant circuit with parasitic resistances. The optimal inductive and resistive loads are found for the power produced from harmonic pressure ripple excitation. Parameters affecting the power response versus the excitation frequency are discussed in detail. The model is validated using prototypes that were developed and tested. Two of the HPEH prototypes demonstrate milli-Watt level average power. Highest normalized power density is reported for the single-crystal prototype. Future work involves further testing of the optimal resistive and inductive loads, in addition to other piezoelectric parameters related to the power response. Also, analysis and testing of power conditioning for HPEH devices are planned.

Acknowledgements

A number of undergraduates worked on this project to develop the HPEH prototypes, including Jeremy Savor, Nalin Verma, Chong Woo Han, and Karthika Poonammalle Venkatasubramanian for the specific prototypes analyzed in this paper. This research was supported in part by the Center for Compact and Efficient Fluid Power, a National Science Foundation Engineering Research Center funded under cooperative agreement number EEC-0540834.

References

[1] Cunefare K A *et al* 2013 Energy harvesting from hydraulic pressure fluctuations *Smart Mater. Struct.* **22** 025036
[2] Anton S R and Sodano H A 2007 A review of power harvesting using piezoelectric materials (2003-2006) *Smart Mater. Struct.* **16** R1–21
[3] Beeby S P, Tudor M J and White N M 2006 Energy harvesting vibration sources for microsystems applications *Meas. Sci. Technol.* **17** R175–95
[4] Cook-Chennault K A, Thambi N and Sastry A M 2008 Powering MEMS portable devices—a review of non-regenerative and regenerative power supply systems with special emphasis on piezoelectric energy harvesting systems *Smart Mater. Struct.* **17** 043001
[5] Kim H *et al* 2007 Consideration of impedance matching techniques for efficient piezoelectric energy harvesting *IEEE Trans. Ultrason. Ferroelectrics Freq. Control* **54** 1851–9
[6] Taylor R *et al* 2004 Technology development for electromechanical acoustic liners *Int. Symp. on Active Control of Sound and Vibration (Williamsburg, VA)* paper a04_093
[7] Liu F *et al* 2008 Acoustic energy harvesting using an electromechanical Helmholtz resonator *J. Acoust. Soc. Am.* **123** 1983–90
[8] Phipps A *et al* 2009 Demonstration of a wireless, self-powered, electroacoustic liner system *J. Acoust. Soc. Am.* **125** 873–81
[9] Wang D A and Liu N Z 2011 A shear mode piezoelectric energy harvester based on a pressurized water flow *Sensors Actuators* A **167** 449–58
[10] Deterre M, Lefeuvre E and Dufour-Gergam E 2012 An active piezoelectric energy extraction method for pressure energy harvesting *Smart Mater. Struct.* **21** 85004–12
[11] Hagood N W and von Flotow A 1991 Damping of structural vibrations with piezoelectric materials and passive electrical networks *J. Sound Vib.* **146** 243–68
[12] Fleming A J, Behrens S and Moheimani S O R 2000 Synthetic impedance for implementation of piezoelectric shunt-damping circuits *Electron. Lett.* **36** 1525–6
[13] Renno J M, Daqaq M F and Inman D J 2009 On the optimal energy harvesting from a vibration source *J. Sound Vib.* **320** 386–405
[14] Erturk A and Inman D J 2009 An experimentally validated bimorph cantilever model for piezoelectric energy harvesting from base excitations *Smart Mater. Struct.* **18** 025009
[15] DuToit N E and Wardle B L 2007 Experimental verification of models for microfabricated piezoelectric vibration energy harvesters *AIAA J.* **45** 1126–37
[16] Erturk A, Hoffmann J and Inman D 2009 A piezomagnetoelastic structure for broadband vibration energy harvesting *Appl. Phys. Lett.* **94** 254102
[17] Stanton S C, McGehee C C and Mann B P 2009 Reversible hysteresis for broadband magnetopiezoelastic energy harvesting *Appl. Phys. Lett.* **95** 174103
[18] Verma N, Skow E, Cunefare K A and Erturk A 2013 Power density performance improvements for high pressure ripple energy harvesting *Proc. of the ASME 2013 Conf. on Smart Materials, Adaptive Structures and Intelligent Systems* SMASIS2013-3179